



**HAL**  
open science

# Cyclic deformation of TiAl generic microstructures at room and high temperature: Bauschinger effect & strain rate sensitivity

Pierre Serrano, Louise Toualbi, Pascale Kanoute, Alain Couret

## ► To cite this version:

Pierre Serrano, Louise Toualbi, Pascale Kanoute, Alain Couret. Cyclic deformation of TiAl generic microstructures at room and high temperature: Bauschinger effect & strain rate sensitivity. 2019. hal-02386237v1

**HAL Id: hal-02386237**

**<https://hal.science/hal-02386237v1>**

Preprint submitted on 29 Nov 2019 (v1), last revised 10 Jul 2020 (v2)

**HAL** is a multi-disciplinary open access archive for the deposit and dissemination of scientific research documents, whether they are published or not. The documents may come from teaching and research institutions in France or abroad, or from public or private research centers.

L'archive ouverte pluridisciplinaire **HAL**, est destinée au dépôt et à la diffusion de documents scientifiques de niveau recherche, publiés ou non, émanant des établissements d'enseignement et de recherche français ou étrangers, des laboratoires publics ou privés.

# Cyclic deformation of TiAl generic microstructures at room and high temperature: Bauschinger effect & strain rate sensitivity.

P. Serrano<sup>a,\*</sup>, L. Toualbi<sup>a</sup>, P. Kanoute<sup>a</sup>, A. Couret<sup>b</sup>

<sup>a</sup>*Onera - The French Aerospace Lab, Département Matériaux et Structures, F-92322 Châtillon, France*

<sup>b</sup>*CNRS, CEMES (Centre d'Elaboration de Matériaux et d'Etudes Structurales), BP 94347, 29 rue J. Marvig, F-31055 Toulouse, France*

---

## Abstract

The cyclic deformation of four TiAl common microstructures is studied experimentally at room and high temperature. Multilevel and multirate tests are performed to highlight the microstructure impact on the Bauschinger effect and the strain rate sensitivity. The mechanical behaviors are linked to their corresponding deformation mechanisms. Results can directly be used to develop microstructure-sensitive modeling of the mechanical behaviors of TiAl alloys.

*Keywords:* A. Intermetallics (aluminides), B. Cyclic plasticity, B. Plastic deformation mechanisms, D. Microstructure, E. Yield behavior, F.

Mechanical testing

---

---

\*Corresponding author

*Email address:* pierre.serrano@onera.fr (P. Serrano)

## 1. Introduction

Technological advances in aircraft engine design require the use of lightweight materials at increasingly high temperatures. Therefore, intermetallics titanium aluminide alloys based on  $\gamma$ -TiAl have been introduced in the most recent civil turbo-engines as low pressure turbine blades [1]. To extend the use of this material to other application technologies, new alloys are being developed with enhanced mechanical properties [2].

Recently, it has been shown that a significant Bauschinger effect occurs at room temperature on TiAl alloy upon strain reversal loading [3]. Even if this effect has been mentioned in some works [4, 5], few hysteresis loops analysis are available. It can even be stated that the link between the microstructure and the mechanical behavior is mostly understood upon uniaxial and monotonic loadings [6, 7, 8, 9].

Indeed, the thermomechanical behavior of TiAl alloys has been studied only on already optimized microstructures with balanced properties [10, 11, 12]. In [13], a comparison is made between a near- $\gamma$  microstructure and a lamellar microstructure but tests are only performed at room temperature. Other works discuss the cyclic behavior but only by means of the stress or strain amplitude evolution [14, 5, 15, 16, 17]. On cited works, neither the Bauschinger effect nor the strain rate sensitivity were studied.

Hysteresis loop analysis give additional information on the link between the macroscopic behavior and microstructural mechanisms [18]. Moreover, such results are extremely valuable to develop refined plasticity theory as new field of integrated computational materials engineering can help material design [19].

26 The aim of this work is to study the link between TiAl microstructures  
 27 and their corresponding mechanical behavior. Four generic TiAl microstruc-  
 28 tures are studied to correlate the macroscopic behavior to the corresponding  
 29 microstructural mechanisms. Emphasis is made on the Bauschinger effect  
 30 and the strain rate sensitivity. Results can directly be used to develop new  
 31 microstructure-sensitive models to describe the mechanical behavior of TiAl  
 32 alloys.

## 33 2. Material and methods

### 34 2.1. Microstructures

35 The material used is the G4 alloy (Ti-47Al-1Re-1W-0.2Si (at.%)) developed  
 36 at the Onera and obtained via the powder metallurgy route [20]. The ingots  
 37 have been casted at Howmet Casting facilities and the powder produced by  
 38 argon gas atomization at Crucible Industries. Hot Isostatic Pressing (HIP)  
 39 was performed by Bodycote at 140 MPa for 4h at 1250 °C. The chemical  
 40 analysis of the powder compacts is given in Table 1.

Ti (at. %)	Al (at. %)	Re (at. %)	W (at. %)	Si (at. %)	C (ppm)	O (ppm)
50.85	47.01	0.95	0.95	0.24	175	1240

**Table 1.** Chemical composition of the studied G4 alloy.

41 Cylindrical blank were machined from the powder compacts. Heat treat-  
 42 ments were directly applied on those specimens to control the microstructure.  
 43 Temperature induced porosity (TIP) is observed after the treatments be-  
 44 cause of gas entrapped inside the powder after the atomization. The same  
 45 observations as in [21] were made : the occurrence of TIP after temperature

46 annealing depends on the grain size and the annealing time. TIP reduces  
47 drastically fatigue lifetime. However, in our case they have no impact on the  
48 macroscopic mechanical behavior and the hysteresis loop shape because of  
49 their low volume fraction ( $< 1\%$  for all microstructures) [22].

50 For microscopic observations, samples were ground with a series of emery  
51 papers, then polished with colloidal silica paste abrasives down to  $0.25\ \mu\text{m}$ .  
52 Microstructures were examined with a scanning electron microscope (SEM)  
53 by back scattered electron images (BSE). Microstructural parameters were  
54 quantified by image segmentation using ImageJ, a Java-based image processing  
55 program [23]. The apparent surface of grains was measured. The grain  
56 size is taken as the equivalent diameter of the measured shape. Series of  
57 micrographs were examined to ensure that the observations were statistically  
58 representatives. The lamellae spacing was measured following the methodology  
59 proposed in [24] for two types of cooling heat treatments: furnace and air  
60 cooling. The sample was cut in half and the apparent lamellar spacing and  
61 angle were measured on both side after polishing. A stereological correction is  
62 then applied to access the real lamellar spacing. Again, series of measurements  
63 were made to ensure that the observations were statistically representatives.

64 SEM images of the studied microstructures are shown in Fig. 1. The  
65 post-HIP microstructure is a near- $\gamma$  microstructure (Fig. 1a) that contains  
66 mainly small equiaxed  $\gamma$  grains with a mean size of  $5\ \mu\text{m}$ . Smaller  $\beta_0$  ( $\sim$   
67  $2.5\%$ ) and  $\alpha_2$  ( $\sim 2.5\%$ ) equiaxed grains are also observed with a mean size  
68 of  $2\ \mu\text{m}$ .

69 The duplex microstructure (Fig. 1b) is obtained following a heat treatment  
70 at  $1340\ ^\circ\text{C}$  during 4 hours followed by an air cooling. This microstructure

71 contains equiaxed  $\gamma$  grains ( $\sim 5 \mu\text{m}$ ) and lamellar colonies ( $\sim 15 \mu\text{m}$ ). The  
72 grains are surrounded by borders consisting of  $\gamma$  phase and  $\beta_0$  precipitates as  
73 observed in the IRIS alloy [25].

74 The near-lamellar microstructure (Fig. 1c) is obtained following a heat  
75 treatment at  $1360 \text{ }^\circ\text{C}$  during 1 hour followed by an air cooling. This mi-  
76 crostructure contains mainly relatively small lamellar colonies ( $\sim 90 \%$ ,  $\sim 50$   
77  $\mu\text{m}$ ). Some equiaxed  $\gamma$  grains ( $\sim 10 \%$ ,  $\sim 8 \mu\text{m}$ ) are still present. All phases  
78 are surrounded by borders again.

79 Finally, the lamellar microstructure (Fig. 1d) is obtained following a  
80 heat treatment at  $1370 \text{ }^\circ\text{C}$  during 1 hour with a furnace cooling. This  
81 microstructure contains large lamellar grains ( $\sim 200 \mu\text{m}$ ) surrounded by  
82 the border phase. The results of the microstructural characterization are  
83 given in Table 2.

84 It has to be noticed that getting accurate measurements of the TiAl  
85 microstructural attributes is difficult even by Electron BackScatter Diffraction  
86 (EBSD) because of the lamellae size and the pseudo-symmetry of the  $\gamma$ -phase.  
87 For our case, statistical measurement performed by hand was find to be the  
88 most relevant method.

## 89 *2.2. Mechanical testing*

90 For mechanical testing, cylindrical specimens were machined with the  
91 geometry specified in Fig. 2. As described in [14], the size of the gauge  
92 section was optimized to ensure that it contains at least 250 grains for every  
93 investigated microstructure. Room temperature and high temperature tests at  
94  $750 \text{ }^\circ\text{C}$  were conducted in air atmosphere using a MTS servohydraulic machine.  
95 Tests were performed under controlled total strain. Extensometers attached

	$\gamma$		$\alpha_2$		$\beta_0$		$\alpha_2 + \gamma$		
	VF	GS	VF	GS	VF	GS	VF	GS	LS
	(%)	( $\mu\text{m}$ )	(%)	( $\mu\text{m}$ )	(%)	( $\mu\text{m}$ )	(%)	( $\mu\text{m}$ )	( $\mu\text{m}$ )
Near- $\gamma$	95	5	2.5	2	2.5	2	-	-	-
Duplex	50	8	-	-	-	-	50	15	0.08
Near-lamellar	10	8	-	-	-	-	90	50	0.08
Lamellar	-	-	-	-	-	-	100	200	0.3

**Table 2.** Results of the microstructural characterization. VF stands for Volume Fraction, GS stands for Grain Size, LS stands for Lamellae Size.

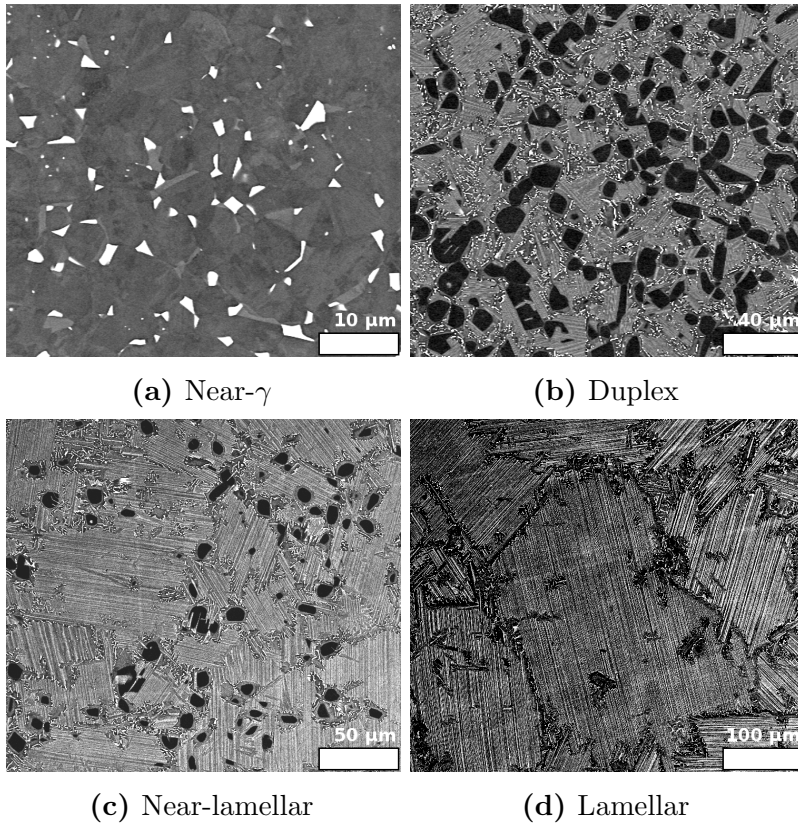


**Fig. 1.** SEM micrographs of the generic microstructures studied in this work.

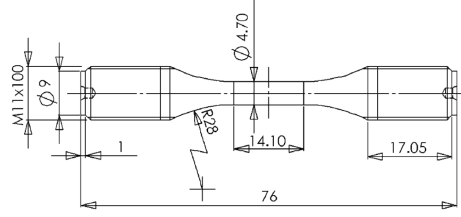


**Fig. 2.** Test specimen geometry.

96 directly to the gauge part of the specimens were used. High temperature tests  
 97 were performed using a furnace monitored by three thermocouples attached  
 98 to the specimen.

99 At both room temperature and 750 °C, a tensile test is first performed.  
 100 Results were used to determine appropriate strain range level for each mi-  
 101 crostructure and to compare monotonic and cyclic behaviors. The strain rate  
 102 at room temperature is  $\dot{\epsilon} = 10^{-3} \text{ s}^{-1}$ . At 750 °C, the viscous behavior was  
 103 investigated by changing the strain rate to  $\dot{\epsilon} = 10^{-5} \text{ s}^{-1}$  during the test, then  
 104 by stopping the test at  $\epsilon = 0.8 \%$  and performing a 8 hours relaxation to  
 105 study the mechanical behavior upon very low strain rate.

106 Multilevel cyclic tests were performed in symmetric tension-compression  
 107 cycle ( $R_{\epsilon} = -1$ ) at  $\dot{\epsilon} = 10^{-3} \text{ s}^{-1}$  for room temperature tests and multiple  
 108 strain rates for high temperature tests. Strain range levels were defined  
 109 based on tensile test results. This type of cyclic tests highlights the major  
 110 characteristics of the mechanical behavior with a limited number of specimens  
 111 and is suited to the development of refined plasticity theories.

### 112 2.3. Bauschinger effect analysis

113 The mechanical behavior of material upon strain reversal loading is usually  
 114 characterized by the Bauschinger effect, defined as a reduction of the yield



115 stress upon load reversal [26]. A scheme showing the typical stress-strain  
116 behavior under strain controlled symmetric tension-compression tests is shown  
117 in Fig. 3. Quantities detailed below are measured and used to discuss the  
118 microstructure influence on this effect.

119 For tensile test and the first cycle of cyclic tests, the yield stress  $\sigma_0$  and  
120 0.2 % yield stress  $\sigma_{0.2\%}$  are respectively defined as the lowest stress point at  
121 which permanent deformation can be measured and the stress at 0.2 % plastic  
122 strain. A Bauschinger effect is observed if the compressive yield stress  $\sigma_c$  is  
123 lower than the yield stress such that  $|\sigma_c| < |\sigma_0|$ . This effect can be caused by  
124 different phenomena.

125 It has been stated that in the case of TiAl alloys, the Bauschinger effect is  
126 mainly caused by a significant transient softening [3]. This transient softening  
127 can be seen as a decrease of the initial elastic domain  $ED_0$  defined as  $ED_0 =$   
128  $2\sigma_0$ , that becomes  $ED_C$  upon load reversal [27, 28]. The transient softening  
129 can therefore be quantified as  $TS_{OC} = ED_0 - ED_C$ .

130 Even in the case where  $ED_0 = ED_C$ , a Bauschinger effect is still observed  
131 if there is kinematic hardening. This is defined as the displacement of the  
132 initial elastic domain center, the point  $A$  on the scheme, that becomes point  
133  $B$  upon load reversal. This leads once again to a lower compressive yield  
134 stress  $\sigma_c$  as  $|\sigma_c| < |\sigma_0|$ .

135 Cyclic plasticity experiments with  $R_\epsilon = -1$  can also reveal a tension-  
136 compression asymmetry [29]. Such asymmetry is usually discussed by studying  
137 the difference between the stress at the maximal peak strain  $\sigma_1$  and the stress  
138 at the minimal peak strain,  $\sigma_2$ . Another interesting way to reveal a tension-  
139 compression asymmetry is to compare the size of the elastic domain upon

140 compression,  $ED_C$ , to the size of the elastic domain upon tension,  $ED_T$ .

141 It should be noted that the Bauschinger effect can also be caused by  
 142 a permanent softening, which is defined by a loss of strength between the  
 143 forward and reverse parts of the test [30]. As it has already been shown that  
 144 it does not happen in the case of TiAl alloys in [3], it will not be mentioned  
 145 thereafter.

146 Finally, the evolution of the elastic domains, the peak stresses and the  
 147 hysteresis loop shapes over the course of the test are studied to get insight  
 148 over a potential cyclic hardening or softening.

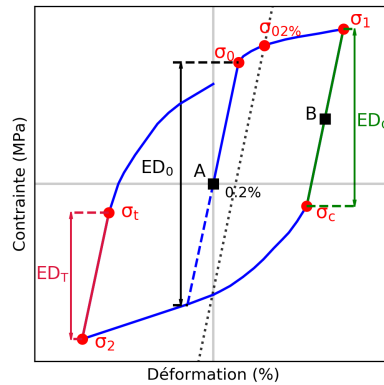


**Fig. 3.** Cyclic stress-strain behavior scheme.  $\sigma_0$  is the yield stress,  $\sigma_{0.2\%}$  the 0.2% yield stress,  $\sigma_1$  and  $\sigma_2$  are the stresses respectively at the maximum and minimum peak strain,  $\sigma_C$  and  $\sigma_T$  are respectively the compressive and tensile yield strength during a fully reversed cycle.  $ED_0$ ,  $ED_C$  and  $ED_T$  are respectively, the initial elastic domain, the compressive elastic domain and the tensile elastic domain. Points A and B are the centers of their corresponding elastic domains.

### 149 **3. Results**

#### 150 *3.1. Room temperature tests*

151 Room temperature tensile properties are illustrated in Fig. 4. The ductility  
152 is limited regardless of the microstructure. The microstructures exhibit various  
153 behavior. The near- $\gamma$  shows the highest stress state with an initial bump. The  
154 duplex microstructure shows a steep entry in plasticity and linear hardening.  
155 For the near-lamellar and the lamellar microstructure the elastic-plastic  
156 transition is smoother. Their yield stresses are equals, but differences in  
157 hardening led to different  $\sigma_{0.2\%}$ .

158 Multilevel cycle tests were designed to study the elastic-plastic transition  
159 by performing 5 cycles at  $\Delta\varepsilon = 0.1\%$ , 5 cycles at  $\Delta\varepsilon = 0.2\%$  and cycles  
160 up to specimen failure at  $\Delta\varepsilon = 0.4\%$ . Results are shown in Fig. 5. Poor  
161 powder quality induced failure after a small number of cycles, but enough  
162 were performed to analyze the cyclic stress strain behavior.

163 For all microstructures, the mechanical behavior during the first strain  
164 range level is elastic as no permanent strain is observed and  $\sigma_0$  is not reached.  
165 The initial elastic domain is therefore clearly defined by  $ED_0 = 2\sigma_0$ . Then, a  
166 typical Bauschinger effect is observed for all microstructure after the onset  
167 of plasticity. This effect is mainly caused by a significant transient softening  
168 (i.e.  $ED_0$  is reduced to  $ED_C$  and  $ED_T$  (see section 2.3)) but a kinematic  
169 hardening is also observed. The stabilized hysteresis loop is immediately  
170 reached as only the level transition cycles (dashed lines on the figures) are  
171 different from the others. Almost no cyclic hardening or softening are observed  
172 for all microstructures and there is no modification of the loop shapes until  
173 failure. When comparing the near-lamellar and lamellar microstructures, it

174 can observed that plasticity starts in both cases at  $\Delta\varepsilon/2 = 0.2 \%$  as the yield  
175 stress are the same, but that the hysteresis loop is more open for the lamellar  
176 microstructure.

177 To discuss the Bauschinger effect causes, the stress is plotted as a function  
178 of the plastic strain for the stabilized hysteresis loops corresponding to  
179  $\Delta\varepsilon/2 = 0.4 \%$  in Fig. 6a. The kinematic hardening observed for the near-  
180 lamellar microstructure is more pronounced than the one of the lamellar  
181 microstructure. Indeed, for both microstructures, the initial elastic domains  
182  $ED_0$  and their associated centers are identical. But it can be observed in  
183 Fig. 6a that at  $\Delta\varepsilon/2 = 0.4 \%$ , the elastic domain center of the near-lamellar  
184 microstructure is now at a higher position than the one of the lamellar  
185 microstructure.

186 The elastic domain sizes can be easily measured from those hysteresis loops,  
187 as they correspond to the stress range for which no plastic strain occurs. The  
188 elastic domain sizes upon compressive and tensile stress ( $ED_C$  and  $ED_T$ ) are  
189 measured, and the transient softening is quantified as  $TS_{OC} = ED_0 - ED_C$   
190 and  $TS_{OT} = ED_0 - ED_T$ . The evolution of the elastic domains size and  
191 transient softening as a function of the  $\gamma$  phase volume fraction are shown in  
192 Fig. 6b.

193 The transient softening increases dramatically with the  $\gamma$  phase volume  
194 fraction. The comparison between the elastic domain sizes upon compressive  
195 and tensile stress reveals a pronounced tension-compression asymmetry for  
196 the two microstructures that contains a significant  $\gamma$  phase volume fraction.  
197 Regarding both lamellar microstructures, their elastic domain sizes and  
198 transient softenings are equals.

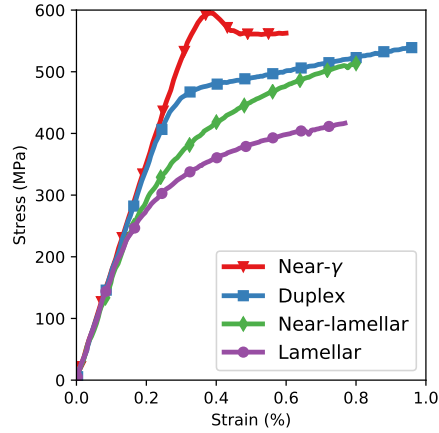


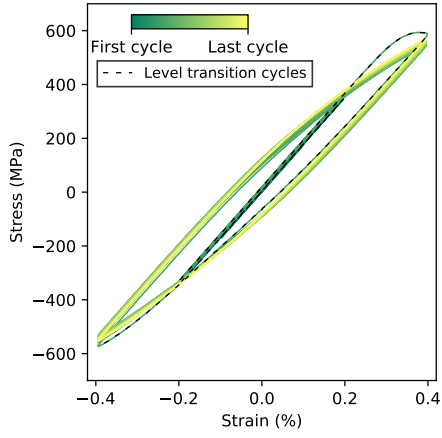
**Fig. 4.** Tensile curves at room temperature,  $\dot{\varepsilon} = 10^{-3} \text{ s}^{-1}$ .

199 *3.2. High temperature tests*

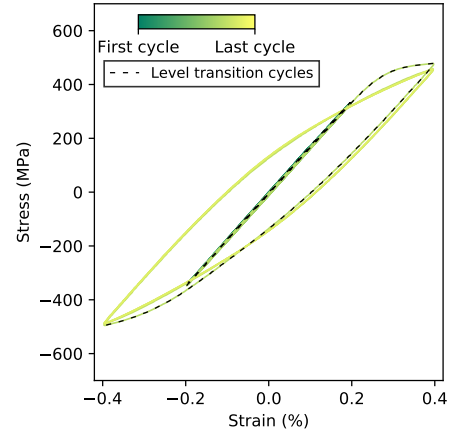
200 Tensile tests at two strain rates followed by a 8 hours relaxation were  
 201 performed at 750 °C. The results are shown in Fig. 7. The strain rate  
 202 modification was made at  $\varepsilon = 0,4 \%$  and  $\varepsilon = 0.6 \%$  based on the results at  
 203 room temperature to avoid early failure (see Fig. 7a).

204 The behavior is now ductile. A decrease of the mechanical properties  
 205 (Young modulus, yield stresses) is observed compared to room temperature  
 206 tests. Nevertheless, the microstructure strength hierarchy is the same, and  
 207 the observations made regarding the plasticity and hardening behavior are  
 208 still true. It is not possible to say if the bump on the near- $\gamma$  microstructure  
 209 has disappeared, as it might have occurred simultaneously with the first strain  
 210 rate change.

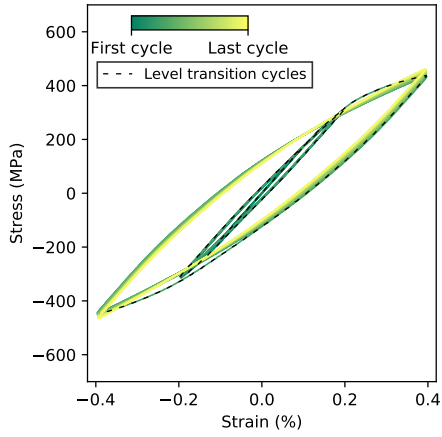
211 The strain rate modification reveals the microstructure impact on the  
 212 viscosity. The strain rate sensitivity is discussed through the stress gap  
 213 that occurs during the strain rate modification. The near- $\gamma$  microstructure  
 214 presents the most viscosity effects, followed by the duplex. The near-lamellar



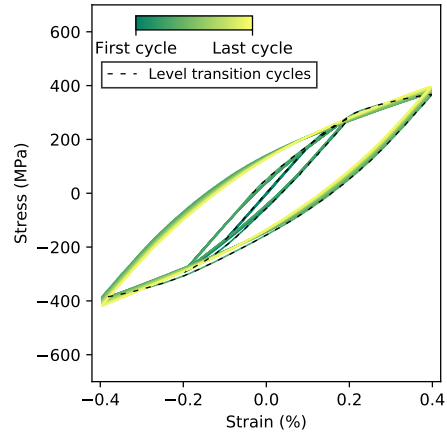
(a) Near- $\gamma$



(b) Duplex

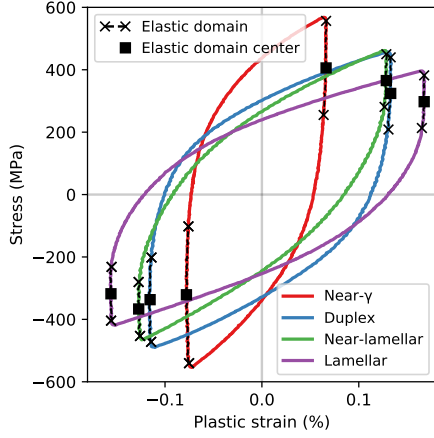


(c) Near-lamellar

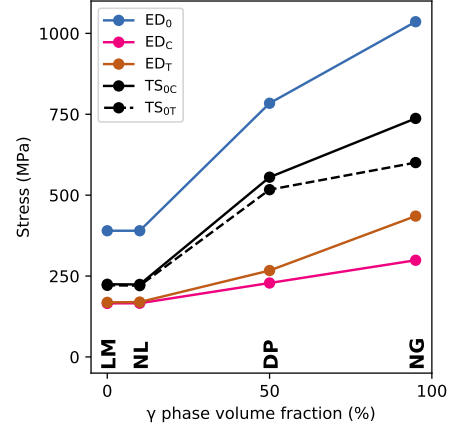


(d) Lamellar

**Fig. 5.** Room temperature multilevel cyclic tests results.



(a) Hysteresis loops for  $\Delta\varepsilon = 0.4\%$ .



(b) Elastic domain evolution.

**Fig. 6.** Bauschinger effect analysis at room temperature. NG, DP, NL and LM respectively stand for Near- $\gamma$ , Duplex, Near-lamellar and Lamellar microstructure. (For interpretation of the references to color in this figure legend, the reader is referred to the Web version of this article.)

215 and lamellar microstructures show almost no strain rate sensitivity. During  
 216 the 8 hours relaxation, the mechanical behavior upon very low strain rate is  
 217 revealed (Fig. 7b). The lamellar microstructure shows low relaxation whereas  
 218 the near-lamellar has almost the same behavior as the duplex and near- $\gamma$   
 219 microstructure. Therefore, a small amount of globular  $\gamma$  phase on a TiAl  
 220 microstructure significantly modifies the low strain rate mechanical behavior.

221 Multilevel and multistrain cyclic tests are conducted in tension-compression  
 222 under strain controlled at 750 °C. At each strain amplitude, 64 cycles are per-  
 223 formed at a strain rate  $\dot{\varepsilon} = 10^{-3} \text{ s}^{-1}$ , 32 at  $\dot{\varepsilon} = 10^{-4} \text{ s}^{-1}$  and 8 at  $\dot{\varepsilon} = 10^{-5} \text{ s}^{-1}$ .  
 224 Successive strain amplitudes were defined to get enough data from each mi-  
 225 crostructure based on their room temperature and high temperature tensile  
 226 test results to avoid early failure. The amplitudes are 0.4 %, 0.6 %, 0.8 %

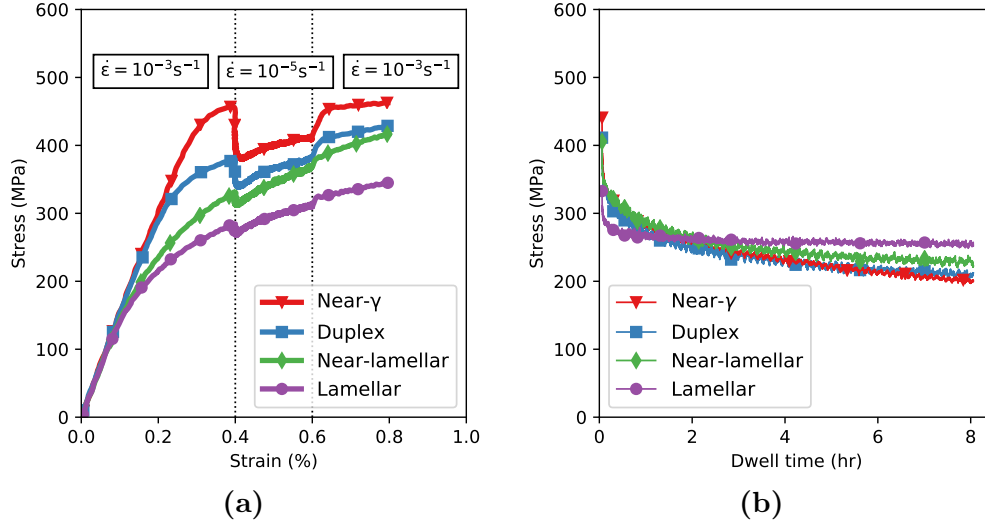


**Fig. 7.** High temperature tensile tests at two strain rates (a) follow by an 8 hours relaxation (b).

227 and 1 % for the near- $\gamma$  and duplex microstructures. The amplitudes are 0.2  
 228 %, 0.4 %, 0.6 % and 0.8 % for the near-lamellar and lamellar microstructures.  
 229 Results are shown in Fig. 8.

230 Once again, stabilized cycle is reached immediately and the strain rate  
 231 sensitivity increases with increasing  $\gamma$  phase volume fraction. For the near- $\gamma$   
 232 microstructure, an important initial transient softening is observed. This  
 233 might indicate that the mechanisms responsible for the bump at room tem-  
 234 perature are still activated at 750 °C as shown by the zoom in Fig. 8a. No  
 235 cyclic hardening or softening was observed regardless of the microstructure.

236 As for the room temperature results, the stress as a function of the plastic  
 237 strain for the stabilized  $\Delta\epsilon/2 = 0.6$  % hysteresis loops and the evolution of  
 238 the elastic domain sizes are studied. The results are shown in Fig. 9a and  
 239 Fig. 9b. Remarkably, the transient softening observed for each microstructure



240 is almost the same at 750 °C than the one observed at room temperature.  
241 Finally, the tension-compression asymmetry of the near- $\gamma$  microstructure has  
242 decreased and is almost insignificant.

#### 243 4. Discussion

244 At room temperature and 750 °C and for strain rate in the range from  
245  $10^{-3} \text{ s}^{-1}$  to  $10^{-5} \text{ s}^{-1}$ , plastic deformation in TiAl occurs by glide of ordinary  
246 dislocations and twinning [7, 31]. At 750 °C, the deformation is eased by the  
247 activation of cross slip. Based on the experimental results, the mechanical  
248 behavior of TiAl microstructures can be classified in two categories.

249 The first type of behavior corresponds to microstructures with a high  $\gamma$   
250 phase volume fraction, in our case the near- $\gamma$  and duplex. Their behavior is  
251 characterized by a steep entry into plasticity, with an initial bump for the  
252 near  $\gamma$  microstructure, followed by a pronounced transient softening upon  
253 reverse flow stress. The bump phenomena was linked to the activation of the  
254 first twinning systems in [32, 33]. It might be related to the fact that twin  
255 nucleation is more difficult than twin propagation [34]. Detailed TEM and  
256 neutron diffraction investigations during cyclic tests suggest that major twins  
257 are nucleated when the strain range increase, i.e. during the first cycle of  
258 the considered strain range level [35]. This twin nucleation during the first  
259 loading part creates interfaces. TEM investigations and dislocation dynamic  
260 simulations confirmed that those boundaries are obstacles to dislocation  
261 movement, and therefore back stress generators [36, 37]. Furthermore, it was  
262 observed on steel that this back stress do create a significant Bauschinger  
263 effect caused by transient softening [38].

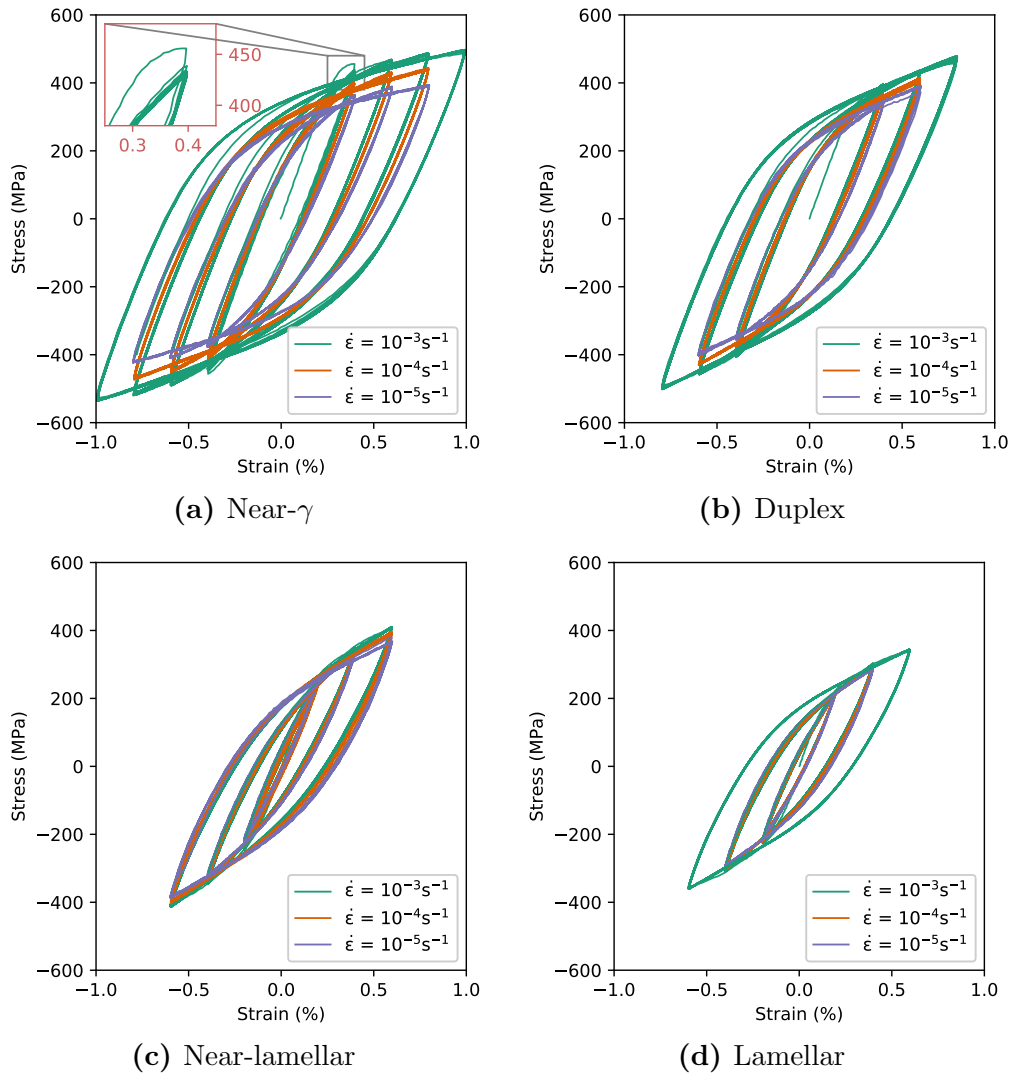
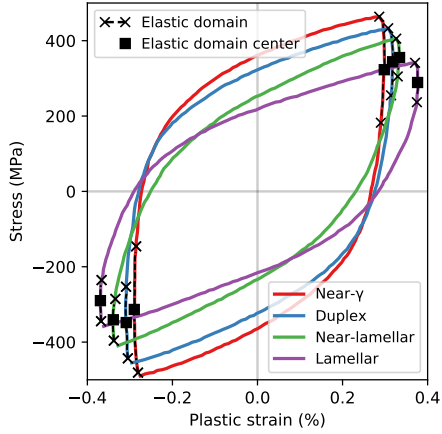
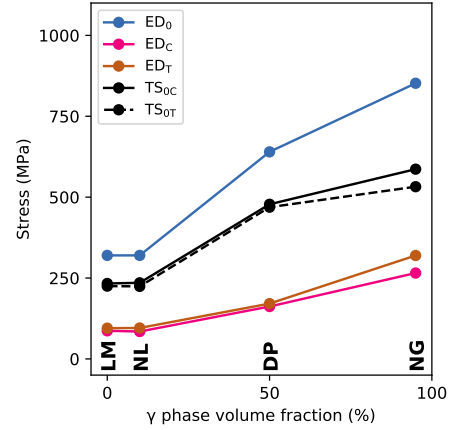


**Fig. 8.** Multilevel and multirate cyclic tests at 750 °C results. (For interpretation of the references to color in this figure legend, the reader is referred to the Web version of this article.)



(a) Hysteresis loops for  $\Delta\varepsilon = 0.6\%$ .



(b) Elastic domain evolution.

**Fig. 9.** Bauschinger effect analysis at 750 °C. NG, DP, NL and LM respectively stand for Near- $\gamma$ , Duplex, Near-lamellar and Lamellar microstructure. (For interpretation of the references to color in this figure legend, the reader is referred to the Web version of this article.)

264 Based on the expensive microstructural analysis available in the literature,  
 265 the following scenario can be defined. Twin are created during the first  
 266 loading part of cyclic tests, therefore creating new boundaries within grains  
 267 and an important back stress when interacting with dislocations. Because the  
 268 shortness of their Burgers vector and since only one twinning dislocation can  
 269 propagate in each plane, twinning is able to bring only a moderate amount  
 270 of strain. Hence, the subsequent strain is largely due to glide of ordinary  
 271 dislocations, the movement of which being impacted by the twins forming  
 272 obstacles to their propagation. During the compression strain application,  
 273 partial back movement of twin dislocations, nucleation and propagation of  
 274 new twinning systems compatible with the compression strain as well as glide  
 275 of ordinary dislocations should be activated. These three kinds of movement

276 are facilitated by the back stress created during the tensile strain, leading to  
277 the tension-compression asymmetry. As a result, a pronounced Bauschinger  
278 effect caused mainly by transient softening is observed during the compression  
279 part. In fact, if another test was performed by starting in compression first,  
280 we suspect that the asymmetry might change direction. When cycling at the  
281 same strain range, ordinary dislocations which are easily able to multiply and  
282 to accommodate both compression and tension strains propagate the applied  
283 deformation. The stress does not increase and therefore the twin network  
284 does not change drastically as twins thicken. Hence, the stabilized cycle is  
285 immediately reached. The same scenario occurs at high temperature. The  
286 bump is only less pronounced as deformation by ordinary dislocations is  
287 eased by the activation of cross slip.

288 The small cyclic hardening observed at room temperature is similar to  
289 the cyclic stress strain behavior that has been observed on an equiaxed  
290 near- $\gamma$  microstructure in [39], but different from the one observed on cast  
291 material for which a significant hardening was observed [13]. That hardening  
292 is usually associated to the formation of a vein-like dislocation structure and  
293 twin-dislocation interactions [5]. The mechanisms responsible for the absence  
294 of cyclic hardening at high temperature are unclear but are most certainly  
295 related to the capability of dislocation to cross-slip, promoting the dislocation  
296 annihilation processes, thus limiting the hardening.

297 The second type of behavior corresponds to microstructures with a high  
298 volume fraction of lamellar colonies. This behavior is characterized by a  
299 smooth entry to plasticity. The two investigated microstructures exhibit the  
300 same yield stresses but different 0.2 % yield stresses. This can be explain by

301 the important plastic anisotropy of lamellar colonies that has been revealed  
302 by studying lamellar single colonies [40]. This anisotropy leads favorably  
303 oriented lamellar colonies to yield well before the macroscopic yield stress  
304 [41, 42]. Therefore when performing tests at the macroscopic scale, the grain  
305 size and lamellae size effects are only observed on the 0.2 % yield stresses  
306 following a Hall-Petch law. This is why in this work, from a macroscopic point  
307 of view, the microstructural attributes affect mostly the kinematic hardening  
308 and not the apparent yield stress.

309 During cyclic tests, a Bauschinger effect caused by transient softening  
310 is observed. The transient softening is far less pronounced than the one of  
311 microstructures with a high volume fraction of  $\gamma$  grains. Nevertheless, TEM  
312 observations suggest that the phenomena causing this softening are most  
313 certainly similar but less striking because of the multiscale aspect of lamellar  
314 microstructures [5]. As the deformation is constrained within lamellae, those  
315 phenomena are not highlighted during macroscopic tests.

316 Regarding the strain rate sensitivity, multirate tensile test results show  
317 that the microstructure sensitivity to viscosity effects increases with the  
318  $\gamma$  grain volume fraction. The relaxation part of the test reveal that the  
319 mechanical behavior upon very low strain rate is drastically modified by  
320 adding a small volume fraction of  $\gamma$  phase. It thus appears that at low strain  
321 rate, the deformation only propagates in the soft  $\gamma$  areas, as in a composite  
322 material made of deformable and undeformable parts. This is an important  
323 observation as near-lamellar microstructures that consists of lamellar colonies  
324 with a fraction of globular  $\gamma$  grains are often considered as the optimal  
325 microstructure in TiAl alloys because of their balanced mechanical properties

326 [43, 25].

## 327 5. Conclusions

328 The mechanical behavior of four generic TiAl microstructures has been  
329 studied at room and high temperature by means of mechanical testing,  
330 including cyclic plasticity experiments. The phenomena observed at the  
331 macroscopic scale are linked with their corresponding microscopic mechanisms.  
332 The mechanical behaviors can be classified in two categories.

333 Microstructures containing an important volume fraction of  $\gamma$  grains  
334 exhibit a pronounced Bauschinger effect caused mainly by a spectacular  
335 transient softening. This sudden softening is attributed to the onset of  
336 twinning and the dislocation-twin interactions. At room temperature, those  
337 microstructures exhibit a tension-compression asymmetry during cyclic tests  
338 that manifests as different elastic domain sizes depending on the flow stress  
339 direction.

340 Microstructure with a high volume fraction of lamellar colonies show  
341 little distinction between the elastic and plastic domains because of the  
342 multiscale aspect of the microstructure and the pronounced plastic anisotropy  
343 of lamellar colonies. A Bauschinger effect is also observed, partly caused by a  
344 transient softening that is far less significant than the one described above, but  
345 mostly due to a pronounced kinematic hardening. At the macroscopic scale,  
346 the impact of the lamellar microstructural attributes appears only on the  
347 kinematic hardening because of the multiscale aspect of the microstructure.

348 At 750 °C, the microstructure strength hierarchy and the observed phe-  
349 nomena are the same than those observed at room temperature. Particularly,

350 the transient softening levels are almost exactly similar to the ones observed  
351 at room temperature. The strain rate sensitivity is shown to increase with  
352 the globular  $\gamma$  phase volume fraction. Relaxation tests revealed that even  
353 a low amount of globular  $\gamma$  grains deeply modifies the mechanical behavior  
354 upon very low strain rate.

355 To conclude, components made in TiAl alloys must be designed carefully as  
356 significant unwanted plasticity might occurs upon strain reversal, particularly  
357 if the mechanical behavior is closed to the one observed for the near- $\gamma$   
358 and duplex microstructures. The given experimental results open a fruitful  
359 opportunity for the development of microstructure-sensitive plasticity theories  
360 and the modeling of TiAl alloys mechanical behavior.

## Acknowledgement

The authors would like to thank our colleagues Camille Liard for performing the experiments and Marc Thomas for providing the material and helpful discussions.

## References

- [1] BP Bewlay, S Nag, A Suzuki, and MJ Weimer. Tial alloys in commercial aircraft engines. *Materials at High Temperatures*, 33(4-5):549–559, 2016.
- [2] Young-Won Kim and Sang-Lan Kim. Advances in gammalloy materials–processes–application technology: successes, dilemmas, and future. *JOM*, 70(4):553–560, 2018.
- [3] Jonathan DH Paul, Roland Hoppe, and Fritz Appel. On the bauschinger effect in tial alloys. *Acta Materialia*, 104:101–108, 2016.

- [4] T Nakano, HY Yasuda, N Higashitanaka, and Y Umakoshi. Anomalous behaviour of cyclic deformation and fatigue properties of tial pst crystals under constant applied stress. *Acta materialia*, 45(11):4807–4821, 1997.
- [5] Anne-Lise Gloanec, Mustapha Jouiad, Denis Bertheau, Marjolaine Grange, and G Hénaff. Low-cycle fatigue and deformation substructures in an engineering tial alloy. *Intermetallics*, 15(4):520–531, 2007.
- [6] Young-Won Kim and Dennis M Dimiduk. Progress in the understanding of gamma titanium aluminides. *Jom*, 43(8):40–47, 1991.
- [7] Fritz Appel, Jonathan David Heaton Paul, and Michael Oehring. *Gamma titanium aluminide alloys: science and technology*. John Wiley & Sons, 2011.
- [8] A Brotzu, F Felli, F Marra, D Pilone, and G Pulci. Mechanical properties of a tial-based alloy at room and high temperatures. *Materials Science and Technology*, 34(15):1847–1853, 2018.
- [9] Hee Y Kim and Soon H Hong. Effect of microstructure on the high-temperature deformation behavior of ti-48al-2w intermetallic compounds. *Materials Science and Engineering: A*, 271(1-2):382–389, 1999.
- [10] Ali El-Chaikh, Thomas K Heckel, and Hans-J Christ. Thermomechanical fatigue of titanium aluminides. *International Journal of Fatigue*, 53:26–32, 2013.
- [11] Stephen-Peter Brookes, H-J Kühn, Birgit Skrotzki, Hellmuth Klingelhöffer, Rainer Sievert, J Pfetzing, D Peter, and G Eggeler. Axial–



- torsional thermomechanical fatigue of a near- $\gamma$  tial-alloy. *Materials Science and Engineering: A*, 527(16-17):3829–3839, 2010.
- [12] Fritz Appel, Thomas K Heckel, and Hans-Jürgen Christ. Electron microscope characterization of low cycle fatigue in a high-strength multiphase titanium aluminide alloy. *International Journal of Fatigue*, 32(5):792–798, 2010.
- [13] Masahide Satoh, Susumu Horibe, Morihiko Nakamura, and Hiroyuki Uchida. Cyclic deformation and fatigue in tial intermetallic compound under plastic strain control. *International Journal of Fatigue*, 32(4):698–702, 2010.
- [14] O Berteaux, M Jouiad, M Thomas, and G Hénaff. Microstructure–low cycle fatigue behaviour relationships in a pm  $\gamma$ -tial alloy. *Intermetallics*, 14(10-11):1130–1135, 2006.
- [15] G Malakondaiah and T Nicholas. High-temperature low-cycle fatigue of a gamma titanium aluminide alloy ti-46al-2nb-2cr. *Metallurgical and Materials Transactions A*, 27(8):2239, 1996.
- [16] Gilbert Hénaff and Anne-Lise Gloanec. Fatigue properties of tial alloys. *Intermetallics*, 13(5):543–558, 2005.
- [17] T Kruml and K Obrtlík. Microstructure degradation in high temperature fatigue of tial alloy. *International Journal of Fatigue*, 65:28–32, 2014.
- [18] Benjamin Fournier, Maxime Sauzay, Christel Caës, Michel Noblecourt, and Michel Mottot. Analysis of the hysteresis loops of a martensitic

- steel: Part i: Study of the influence of strain amplitude and temperature under pure fatigue loadings using an enhanced stress partitioning method. *Materials Science and Engineering: A*, 437(2):183–196, 2006.
- [19] David L McDowell. Microstructure-sensitive computational structure-property relations in materials design. In *Computational Materials System Design*, pages 1–25. Springer, 2018.
- [20] M Grange, JL Raviart, and M Thomas. Influence of microstructure on tensile and creep properties of a new castable tial-based alloy. *Metallurgical and Materials Transactions A*, 35(7):2087–2102, 2004.
- [21] Gerhard Wegmann, Rainer Gerling, and Frank-Peter Schimansky. Temperature induced porosity in hot isostatically pressed gamma titanium aluminide alloy powders. *Acta Materialia*, 51(3):741–752, 2003.
- [22] Nikhilesh Chawla and X Deng. Microstructure and mechanical behavior of porous sintered steels. *Materials Science and Engineering: A*, 390(1-2):98–112, 2005.
- [23] Caroline A Schneider, Wayne S Rasband, and Kevin W Eliceiri. Nih image to imagej: 25 years of image analysis. *Nature methods*, 9(7):671, 2012.
- [24] Olivier Berteaux. *Etude des mécanismes d’écrouissage et d’endommagement cycliques des alliages TiAl élaborés par métallurgie des poudres*. PhD thesis, Poitiers, 2005.
- [25] Thomas Voisin, Jean-Philippe Monchoux, Mickael Perrut, and Alain

- Couret. Obtaining of a fine near-lamellar microstructure in tial alloys by spark plasma sintering. *Intermetallics*, 71:88–97, 2016.
- [26] J Bauschinger. On the change of position of the elastic limit of iron and steel under cyclic variations of stress. *Mitt. Mech.-Tech. Lab., Munich*, 13(1), 1886.
- [27] PB Pragnell, WM Stobbs, and PJ Withers. Considerations in the use of yield asymmetries for the analysis of internal stresses in metal matrix composites. *Materials Science and Engineering: A*, 159(1):51–63, 1992.
- [28] PB Pragnell, T Downes, PJ Withers, and T Lorentzen. An examination of the mean stress contribution to the bauschinger effect by neutron diffraction. *Materials Science and Engineering: A*, 197(2):215–221, 1995.
- [29] BD Smith, DS Shih, and DL McDowell. Cyclic plasticity experiments and polycrystal plasticity modeling of three distinct ti alloy microstructures. *International Journal of Plasticity*, 101:1–23, 2018.
- [30] LM Brown and WM Stobbs. The work-hardening of copper-silica v. equilibrium plastic relaxation by secondary dislocations. *Philosophical Magazine*, 34(3):351–372, 1976.
- [31] Alain Couret. Glide mechanism of ordinary dislocations in the  $\gamma$  phase of tial. *Intermetallics*, 9(10-11):899–906, 2001.
- [32] Florian Kauffmann, Thomas Bidlingmaier, Gerhard Dehm, Alexander Wanner, and Helmut Clemens. On the origin of acoustic emission during room temperature compressive deformation of a  $\gamma$ -tial based alloy. *Intermetallics*, 8(7):823–830, 2000.

- [33] WT Marketz, FD Fischer, and H Clemens. Deformation mechanisms in tial intermetallicsexperiments and modeling. *International Journal of Plasticity*, 19(3):281–321, 2003.
- [34] S Farenc, A Coujou, and A Couret. An in situ study of twin propagation in tial. *Philosophical Magazine A*, 67(1):127–142, 1993.
- [35] Premysl Beran, Milan Heczko, Tomas Kruml, Tobias Panzner, and Steven van Petegem. Complex investigation of deformation twinning in  $\gamma$ -tial by tem and neutron diffraction. *Journal of the Mechanics and Physics of Solids*, 95:647–662, 2016.
- [36] Slim Zghal and Alain Couret. Transmission of the deformation through  $\gamma$ - $\gamma$  interfaces in a polysynthetically twinned tial alloy ii. twin interfaces (180 rotational). *Philosophical Magazine A*, 81(2):365–382, 2001.
- [37] Haidong Fan, Sylvie Aubry, Athanasios Arsenlis, and Jaafar A El-Awady. The role of twinning deformation on the hardening response of polycrystalline magnesium from discrete dislocation dynamics simulations. *Acta Materialia*, 92:126–139, 2015.
- [38] Ibrahim Karaman, Huseyin Sehitoglu, Yu I Chumlyakov, Hans J Maier, and IV Kireeva. The effect of twinning and slip on the bauschinger effect of hadfield steel single crystals. *Metallurgical and Materials Transactions A*, 32(13):695–706, 2001.
- [39] AL Gloanec, G Henaff, M Jouiad, D Bertheau, P Belaygue, and M Grange. Cyclic deformation mechanisms in a gamma titanium aluminide alloy at room temperature. *Scripta materialia*, 52(2):107–111, 2005.

- [40] H Inui, MH Oh, A Nakamura, and M Yamaguchi. Room-temperature tensile deformation of polysynthetically twinned (pst) crystals of tial. *Acta Metallurgica et Materialia*, 40(11):3095–3104, 1992.
- [41] Thomas Edward James Edwards, Fabio Di Gioacchino, Amy Jane Goodfellow, Gaurav Mohanty, Juri Wehrs, Johann Michler, and William John Clegg. Deformation of lamellar  $\gamma$ -tial below the general yield stress. *Acta Materialia*, 163:122–139, 2019.
- [42] R Botten, Xinhua Wu, D Hu, and MH Loretto. The significance of acoustic emission during stressing of tial-based alloys. part i: Detection of cracking during loading up in tension. *Acta materialia*, 49(10):1687–1691, 2001.
- [43] Helmut Clemens and Svea Mayer. Design, processing, microstructure, properties, and applications of advanced intermetallic tial alloys. *Advanced Engineering Materials*, 15(4):191–215, 2013.